

# The Relation Between Line Emission and Brightest Cluster Galaxies in Three Exceptional Clusters: Evidence for Gas Cooling from the ICM

S. L. Hamer<sup>1\*</sup>, A. C. Edge<sup>1</sup>, A. M. Swinbank<sup>1</sup>, R. J. Wilman<sup>2</sup>, H. R. Russell<sup>3</sup>, A.C. Fabian<sup>4</sup>, J.S. Sanders<sup>4</sup> & P. Salomé<sup>5</sup>

<sup>1</sup>*Institute for Computational Cosmology, Department of Physics, University of Durham, South Road, Durham DH1 3LE*

<sup>2</sup>*School of Physics, University of Melbourne, Parkville, Victoria 3010, Australia*

<sup>3</sup>*Department of Physics and Astronomy, University of Waterloo, Waterloo, ON N2L 3G1, Canada*

<sup>4</sup>*Institute of Astronomy, Madingley Road, Cambridge CB3 0HA*

<sup>5</sup>*LERMA, Observatoire de Paris, UMR 8112 du CNRS, 75014, Paris, France*

Accepted TBD; Received TBD; in original form September 2011

## ABSTRACT

There is a strong spatial correlation between brightest cluster galaxies (BCGs) and the peak density and cooling rate of the intra-cluster medium (ICM). In this paper we combine integral field spectroscopy, CO observations and X-ray data to study three exceptional clusters (Abell 1991, Abell 3444 and Ophiuchus) where there is a physical and dynamical offset between the BCG and the cooling peak to investigate the connection between the cooling of the intracluster medium, the cold gas being deposited and the central galaxy. We find the majority of the optical line emission is spatially coincident with the peak in the soft X-rays. In the case of A1991 we make separate detections of CO(2-1) emission on the BCG and on the peak of the soft X-ray emission suggesting that cooling continues to occur in the core despite being offset from the BCG. We conclude that there is a causal link between the lowest temperature (<2 keV) ICM gas and the molecular gas (~30 K). This link is only apparent in systems where a transitory event has decoupled the BCG from the soft X-ray peak. We discuss the prospects for identifying more examples of this rare configuration.

## Key words:

galaxies: clusters: individual: A1991, A3444, Ophiuchus - galaxies: clusters: intra-cluster medium - galaxies: elliptical and cD

## 1 INTRODUCTION

Observations of the central regions of massive galaxy clusters show intense X-ray emission suggesting that the ICM is undergoing significant radiative cooling (Fabian et al. 1981). X-ray emitting gas cools at a rate of  $t_{cool} \propto 1/n$  (where  $n$  is the gas density), suggesting a substantial mass ( $\sim 10^{12} M_{\odot}$ ) of cool gas should be deposited into the central regions and form stars (for a review see Fabian 1994). In typical cases cooling rates of  $50\text{--}100 M_{\odot}\text{yr}^{-1}$  are expected rising as high

as  $>500 M_{\odot}\text{yr}^{-1}$  in the most extreme systems, although sub-mm observations did not detect this gas in molecular form (O’Dea et al. 1994). However, through systematic surveys for CO in clusters, molecular gas masses of  $10^9\text{--}11 M_{\odot}$  have been found (Edge 2001; Salomé & Combes 2003). More recent X-ray observations have revealed much reduced cooling rates ( $\sim 1\text{--}10 M_{\odot}\text{yr}^{-1}$ ) with a sharp truncation in cooling at low (< 1 keV) X-ray temperatures, suggesting a continuous feedback effect is reheating the gas. This heavily suppressed cooling has reduced the large discrepancy between gas deposition rate and observed molecular gas (see the review by Peterson & Fabian 2006).

The clusters X-ray luminosity and temperature re-

\* E-mail: s.l.hamer@durham.ac.uk

late closely to the intrinsic luminosity of the BCG (Schombert 1987, 1988; Edge & Stewart 1991a,b). This connection between the BCG and cluster properties makes BCGs an important tool for studying clusters. Since the dense environment at the centre of clusters means that BCG experiences a much higher ICM pressure than any other cluster member galaxy radiative cooling is at its strongest and gas cooling from the hot phase can be accreted onto the BCG, fuelling its evolution. However, these regions are also densely populated by other galaxies making the likelihood of interactions and mergers much more likely. Both mergers and gas accretion are therefore likely to play important roles in the growth and evolution of the BCG and cluster core (Tremaine 1990; Wilman et al. 2006).

Many BCGs of the most rapidly cooling cluster cores exhibit optical line emission (Cavagnolo et al. 2008). Crawford et al. (1999) found significant line emission in 32 per cent of a sample of 201 BCGs selected from the BCS X-ray selected sample (Ebeling et al. 1998). This line emitting gas at  $10^4$  K traces filamentary structures around the BCG (Hatch et al. 2005, 2006; McDonald et al. 2011) and direct comparison has shown qualitatively similar structures in the  $10^7$  K X-ray (Fabian et al. 2008) and 30 K molecular (Salomé et al. 2011) gas. This structural similarity suggests that the gas phases are linked and as such, studying the line emitting gas can give an insight into the physical mechanisms operating within the cluster cores.

In order to measure the emission line structure of the gas within a more complete sample of clusters we have obtained spatially resolved spectroscopy around the redshifted  $H\alpha$  emission of 77 BCGs (Hamer et al. in preparation). Here, we report observations of three extreme systems (Abell 1991, Abell 3444 and the Ophiuchus cluster) from our parent sample which show a significant component ( $> 50$  per cent) of their line emission significantly offset from the central BCG. A1991 and A3444 are unique from the rest of the sample in that the rest frame optical line emission is significantly offset from the BCG. Figure 1 shows the physical offset between the BCG and the peak  $H\alpha$  emission for the whole sample of 77 line emitting BCGs (Hamer et al. in preparation). It can clearly be seen here that the offsets for the majority of the sample fall below the seeing limit of the VIMOS observations ( $1.5''$ ) with A1991 and A3444 having 9–13 kpc offsets.

We first outline our observations and data reduction (§2) followed by a summary of how we completed our analysis (§3). In §4 we present our results before discussing their implications in §5. Finally a summary and conclusions are reported in §6. We assume  $\Omega_m = 0.27$ ,  $\Lambda = 0.73$  and  $H_o = 71 \text{ km s}^{-1} \text{ Mpc}^{-1}$  throughout. This corresponds to a physical scale of  $1.12 \text{ kpc}''$  for A1991,  $3.91 \text{ kpc}''$  for A3444 and  $0.55 \text{ kpc}''$  for Ophiuchus.

## 2 OBSERVATIONS AND DATA REDUCTION

Observations of the BCG in A1991 were taken using the Visible Multiobject Spectrograph (VIMOS) instrument on the 8.2m Very Large Telescope (VLT) in April

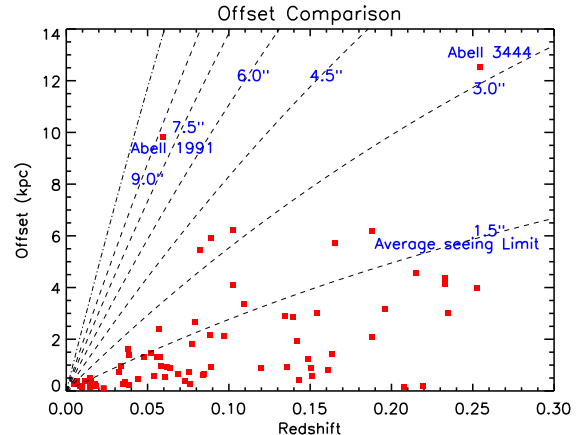


**Figure 1.** Observed physical offset between the BCG and the majority of the line emission in our parent sample of 77 BCGs (Hamer et al. in preparation). The dashed lines show constant offsets in  $1.5''$  steps. The dot-dashed line shows the extent of the VIMOS field of view ( $\sim 12''$  as the BCG was positioned at the centre of the field of view). The majority of objects fall well below the average seeing limit of  $1.5''$  but A1991 and A3444 stand out with offsets of 9–13 kpc.

of 2008 and May of 2010. Observations were made at two positions one centred on the BCG and the second  $\sim 10''$  north of the first to cover the peak in X-ray emission. At both locations a set of three 600 second exposures were performed with a pointing dither included between each exposure to account for bad pixels. The HR\_Orange Grism and GG435 filter (spectral resolution of  $R \sim \Delta\lambda/\lambda \sim 2650$  over the wavelength range 5250–7400 Å) were used to observe  $H\alpha$  ( $\lambda_{\text{rest}} 6562.8 \text{ Å}$ ) at the redshift of the cluster of 0.0587. Observations of A3444 were taken with VIMOS in June 2008 using the HR\_Red Grism and GG475 filter (spectral resolution  $R \sim \Delta\lambda/\lambda \sim 3100$  covering the wavelength range 6450–8600 Å) to observe  $H\alpha$  at the cluster redshift of 0.2533. The observations were taken in a range of conditions, with a seeing of  $\sim 0.7''$ – $1.3''$ .

The raw data were reduced using the *esorex* package. This package performed the basic data reduction including bias subtractions, flat fielding and the wavelength and flux calibrations. To subtract the sky we masked any point-like objects to remove any stars within the field. The BCG was then removed from the field by masking all pixels within an isophote of half its peak intensity. The sky level for each quadrant was then calculated by taking the median value of the remaining pixels at each wavelength increment. This sky spectrum was then subtracted from each pixel in the four quadrants before they were combined into a single datacube. Finally we median combined the three exposures for each pointing in order to eliminate cosmic rays. To mosaic the two positions of A1991 we determine the exact offset between the BCG in both observations and combined them to create a cube with a  $\sim 36'' \times 38''$  field of view.

The Ophiuchus cluster BCG (hereafter Ophiuchus) was observed by Edwards et al. (2009) using Gemini Multi-Object Spectrograph (GMOS) on the 8.1m Gemini

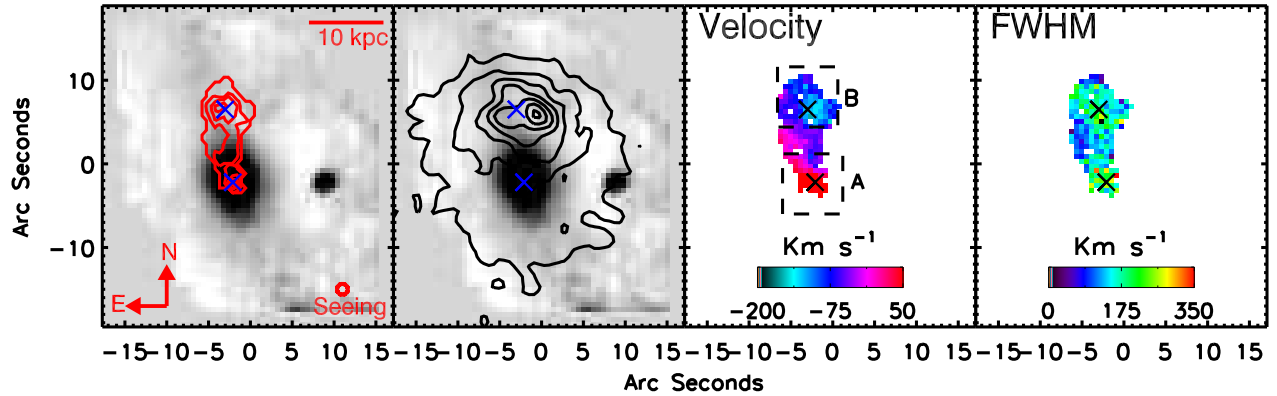


**Figure 2.** *Left:* A continuum image ( $\lambda = 6000\text{--}7000 \text{ \AA}$ ) created from the VIMOS datacube. Overplotted as contours is the  $H\alpha$  emission at 6, 12, 18 and  $24\sigma$  (with  $1\sigma = 9.4 \times 10^{-18} \text{ erg cm}^{-2} \text{ s}^{-1} \text{ arcsec}^{-2}$ ). The  $H\alpha$  emission is double peaked with one component on the BCG but extending north by  $10''$  where a second component can be seen. *Centre-Left:* The continuum image showing the optical stellar component of the BCG with the X-ray map overlaid as contours. The peak in the X-rays is offset by  $\sim 10''$  north of the BCG. *Centre-Right:* The  $H\alpha$  velocity field for A1991, as derived from fits to the  $H\alpha - [\text{NII}]$  complex. The velocities are given relative to a redshift  $z=0.0591$ . *Right:* The FWHM of the  $H\alpha$  line emission deconvolved for instrumental resolution. The crosses mark the location of the two  $H\alpha$  components on each plot. The plots are centred at RA = 14:54:31.567 and Dec = 18:38:32.70 (J2000). There is a component of  $H\alpha$  emission offset to the north of the BCG by  $\sim 10''$  which coincides with the position of the peak in the soft X-ray emission. The velocity gradient along this offset shows a dynamical link still exists between the BCG and the Peak of ICM cooling.

South Telescope (Gemini). This object was selected from the literature as it is the best other example of a BCG showing significant offset between the BCG, the X-ray peak and the line emission (Million & Allen 2009). The observations of Ophiuchus consisted of four 1500 second exposures which were combined to give a total integration time of 6000 seconds. The R400+r grating (spectral resolution  $R \sim \Delta\lambda/\lambda \sim 1918$  covering the wavelength range  $5620\text{--}6980 \text{ \AA}$ ) was used to ensure coverage of  $H\alpha$  at the cluster redshift of 0.0280 (Lahav et al. 1989). The seeing during these observations was  $\sim 0.8''$  to  $1''$ .

The data were reduced using GMOS specific tools in the Gemini IRAF package, which included bias subtraction, flat fielding and wavelength calibration. Sky subtraction was performed by isolating the fibres from a secondary IFU situated  $\sim 1'$  away from the primary IFU. These fibres were then used to create a sky spectrum which was subtracted from the fibres containing the observations. Cosmic rays were then rejected by comparing the spectrum from each fibre to that from neighbouring fibres and rejecting any element which had a value exceeding ten times the Poisson noise. The individual exposures were then combined into a single datacube which covers a region centred on the BCG of  $\sim 5'' \times 7''$ .

We obtained IRAM 30m data for the CO(1-0) and CO(2-1) lines in A1991 on 21st April 2010. The observations were performed in reasonable conditions ( $\tau_{225\text{GHz}} \sim 0.1 - 0.2$ ) with the EMIR receiver using a 4 GHz bandwidth covering each line. Two positions were observed, the BCG and the optical line peak  $11''$  north, each for 1 hour duration with wobbler switching with a  $90''$  throw. The observations reached a noise level of 0.6 mK and 1.3 mK in  $44 \text{ km s}^{-1}$  bins (16 and 32 MHz) for CO(1-0) and CO(2-1) lines respectively. Both the 4 MHz and

Wilma backends were used to sample the data but the noise performance of the 4 MHz backend was considerably better so only the 4 MHz data are presented here.

IRAM 30m observations of CO(1-0) in A3444 were obtained on 29th December 2006, before the VIMOS IFU observations, in very good conditions ( $\tau_{225\text{GHz}} < 0.1$ ) with the A/B100 receivers with a 400 MHz bandwidth for 1 hour duration using wobbler switching with a  $90''$  throw. These observations reached 0.8 mK in  $52 \text{ km s}^{-1}$  bins (16 MHz). At the time of writing, we are aware of no observations of CO in Ophiuchus.

### 3 ANALYSIS

We use the integral field spectroscopy to investigate the spatial variation of line emission and kinematics within the clusters. We fitted gaussian emission line profiles to the region of the spectra containing the  $H\alpha$  ( $\lambda_{\text{rest}} 6562.8 \text{ \AA}$ ) and  $[\text{NII}]$  ( $\lambda_{\text{rest}} 6548.1/6583 \text{ \AA}$ ) in each lenslet. We used a  $\chi^2$  minimisation procedure and allowed the velocity, intensity and linewidth of the  $H\alpha$  line, as well as the continuum level to vary independently. The  $[\text{NII}]$  lines were fixed to the same velocity and linewidth as  $H\alpha$ , the  $[\text{NII}]$  intensity was allowed to vary but the ratio of  $[\text{NII}]6548.1/[\text{NII}]6583$  was fixed to 0.3. The profiles were fitted to each  $0.6''$  pixel and adaptively binned to  $1.8''$  in regions with lower  $H\alpha$  flux. As such the low surface brightness emission has a lower resolution than the brightest regions.

These fits were accepted as representing the data when they provided an improvement over a continuum only fit at the  $7\sigma$  significance level and when an acceptable fit was found the parameters of the best fit model were stored. These parameters were then used to produce

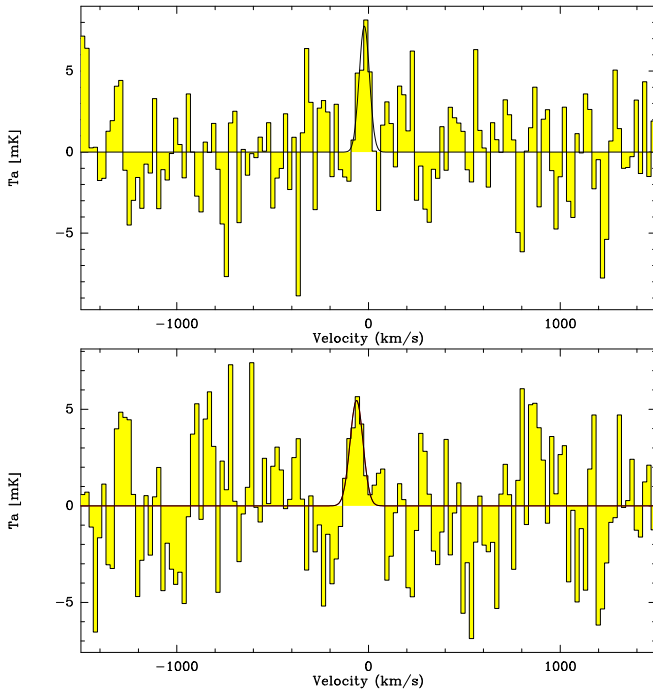


**Figure 3.** *Upper* IRAM 30m EMIR spectrum for A1991 on the BCG. *Lower* IRAM 30m EMIR spectrum for A1991 on the offset optical line peak. The plots show the CO(2-1) line in antenna temperature scale. Significant CO emission is detected at both the position of the BCG ( $3.8\sigma$ ) and the offset H $\alpha$  emission ( $3.0\sigma$ ) and there is a small velocity offset in the line centroid between them.

maps of H $\alpha$  flux, relative velocity and linewidth (FWHM deconvolved for instrumental resolution). Continuum images of the region covered by the observations were also produced by taking the median of the emission from each lenslet over a region of the spectra containing no emission lines or sky line residuals (here after referred to as collapsing the cube).

## 4 RESULTS

### 4.1 Abell 1991

In Figure 2 we show the continuum image of A1991 (collapsed over  $\lambda = 6000\text{--}7000 \text{ \AA}$ ) and overlay contours of H $\alpha$  line emission. It is apparent that while there is a component of the H $\alpha$  emission centred on the BCG a more extended clump is present  $9''$  north lying off the bright stellar component, a projected physical offset of  $\sim 10$  kpc at the cluster redshift of 0.0587 (Struble & Rood 1999).

Table 1 shows the values of the variable parameters for the minimised fits to the emission on the BCG, off the BCG (labelled on Figure 2 as regions A and B respectively) and the emission from the connecting gas. These fits show that the offset clump contains the majority ( $\sim 55$  per cent) of the H $\alpha$  emission within the system.

A1991 also is known to have a significant offset ( $\sim 10''$ ) between the position of the BCG and the X-ray peak (Sharma et al. 2004). Figure 2 shows that the bright peak in the X-ray gas lies roughly  $10''$  (11 kpc) to the

north of the BCG and within 3 kpc of a similar peak in H $\alpha$  emission. This bright X-ray peak corresponds to the lowest temperature gas in the cluster and the region where the gas is cooling most rapidly. This shows that the majority of the H $\alpha$  emitting gas is related to the most rapidly cooling region of the ICM rather than being co-located with the BCG. Analysis of the *Chandra* data indicates that the pressure in the core of the cluster is relatively uniform between the BCG and the cooler, offset peak implying that the enhanced density at the peak is balanced by a lower temperature (Sharma et al. 2004).

In Figure 2 we show the velocity and linewidth maps produced from the fits to the individual lenslets. We note that the velocity map shows a continuous velocity gradient from the position of the BCG along a connecting filament to the offset emission. This suggests that the two components, while physically separated remain kinematically linked. To determine the velocity difference between the two components we extracted spectra from an  $8''$  by  $7''$  aperture centred on the BCG and on the offset component (marked A and B on the velocity map of Figure 2). We find a velocity difference of  $124 \pm 10 \text{ km s}^{-1}$  between the two components. The linewidth (FWHM) of the emission from the BCG is greater ( $205 \pm 9 \text{ km s}^{-1}$ ) than that from the offset component ( $152 \pm 5 \text{ km s}^{-1}$ ).

Next, we combine the H $\alpha$  and the CO properties to investigate the relation between warm and cold gas within the cluster core. By virtue of the good conditions, the relative sensitivity between the two lines with EMIR strongly favours the CO(2-1) line. We obtain a significant detection of it in both positions (Figure 3) of  $3.8\sigma$  on the BCG and  $3.0\sigma$  on the offset line emission. The significance of the line detection was calculated using the variance of the signal away from the line compared to the line strength. By this measure there are two candidate lines at  $-1250$  and  $+930 \text{ km s}^{-1}$  in the offset observation but, if they are real, are unlikely to be related to the BCG.

The separation of the two positions is just smaller than the IRAM beam at this frequency ( $10.3''$  vs  $10.9''$ ) and the measured velocity of the emission is offset by more than half the line width. From the separation and profile of the beam we estimate a less than 10 per cent contamination between the two pointings. Therefore the gas is likely to be spatially extended on a scale comparable, but not necessarily identical to, the optical emission lines. The velocity difference in CO(2-1) between the two positions is  $-40 \pm 20 \text{ km s}^{-1}$  in the same direction as the shift we observe in H $\alpha$  but  $84 \text{ km s}^{-1}$  lower. This difference may be related to the bulk flow of the cold molecular gas or a different overall distribution with respect to the BCG compared to that traced by the optical lines. The significance of this velocity difference and its potential origin are beyond the scope of these single dish observations but could be addressed with deeper interferometry with PdBI or ALMA.

The detection of CO  $10''$  north of the BCG in A1991 makes this the fourth system where extended CO has been found (e.g. NGC1275 Salomé et al. (2006), A1795 Salomé & Combes (2004) and RXJ0821+07 Edge & Frayer (2003)). In all of these systems the extended CO coincides with extended H $\alpha$  emission. Within the system as a whole the implied total molecular gas

TABLE 1.  
 PROPERTIES OF THE ON SOURCE AND OFFSET COMPONENTS

Target	Redshift	Velocity (km s <sup>-1</sup> )	H $\alpha$ Flux (10 <sup>-16</sup> erg cm <sup>-2</sup> s <sup>-1</sup> )	[NII] Flux (10 <sup>-16</sup> erg cm <sup>-2</sup> s <sup>-1</sup> )	Continuum (10 <sup>-16</sup> erg cm <sup>-2</sup> s <sup>-1</sup> Å <sup>-1</sup> )	FWHM (km s <sup>-1</sup> )
Abell 1991						
BCG	0.05935[3]	0 ± 11	10.3 ± 0.7	23.7 ± 0.68	6.41 ± 0.27	205 ± 9
Offset	0.05893[2]	124 ± 10	22.5 ± 1.2	35.1 ± 0.87	0.76 ± 0.41	152 ± 5
Connecting	0.05910[3]	71 ± 11	7.48 ± 0.4	10.1 ± 0.35	2.15 ± 0.19	133 ± 7
Abell 3444						
BCG	0.25583[6]	0 ± 25	15.5 ± 0.7	8.3 ± 0.6	1.0 ± 0.2	490 ± 21
Offset	0.25550[3]	100 ± 19	16.5 ± 0.5	7.8 ± 0.5	< 0.5	273 ± 9
Connection	0.25503[6]	241 ± 26	10.0 ± 0.6	8.2 ± 0.6	0.4 ± 0.2	450 ± 26

**Table 1.** Results from the fit to the H $\alpha$  [NII] triplet for the total spectrum of each object listed. The values in Square brackets are the errors on the last decimal place. For A1991 the BCG emission was defined as coming from a 8'' by 7'' region centred on the on BCG H $\alpha$  peak, shown in Figure 2 as region A, the offset emission was defined in a similar manner about the offset H $\alpha$  peak (region B in Figure 2). Similarly for A3444 the on BCG emission was defined as coming from a 4'' by 5'' region centred on the BCG H $\alpha$  peak and the offset was defined as an equally sized region about the offset H $\alpha$  peak (region A and B in Figure 4 respectively). For both objects the connection is defined as the emission which was not in these previous two regions and consists of the low surface brightness emission joining the two peaks.

 TABLE 2.  
 PROPERTIES OF THE CO(2-1) LINE IN A1991

Target	Significance Sigma( $\sigma$ )	CO(2-1) Line Intensity (K km s <sup>-1</sup> )	Velocity (km s <sup>-1</sup> )	Line width (km s <sup>-1</sup> )	Peak intensity T <sub>mb</sub> (mK)	H <sub>2</sub> gas mass (10 <sup>8</sup> M <sub>⊙</sub> )
On BCG	3.8	0.52±0.16	-22±10	60±18	7.8±2.2	9.9±3.0
Offset	3.0	0.46±0.19	-62±17	79±35	5.5±1.8	8.8±3.6

**Table 2.** CO(2-1) line parameters for the IRAM 30m EMIR observations corrected for beam efficiency. The equivalent analysis for the data for CO(1-0) finds an upper limit of <0.15 K km s<sup>-1</sup> which is consistent with the CO(2-1) detection given the observed range of line intensities for these lines in cluster cores (Edge 2001, Salomé & Combes 2003).

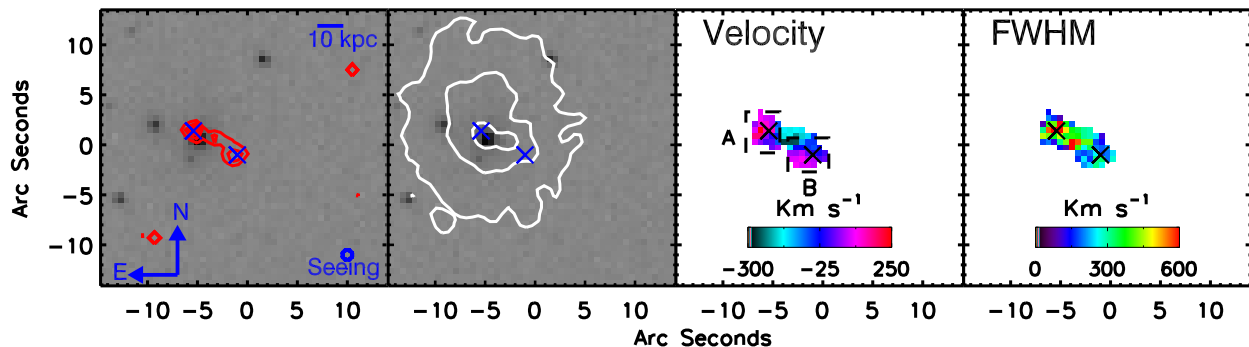


**Figure 4.** *Left:* This shows a FORS2 R band image of the central region of A3444. Overplotted as contours is the H $\alpha$  line emission at 6,12,18 and 24  $\sigma$  (with 1  $\sigma$  = 0.021 × 10<sup>-16</sup> erg cm<sup>-2</sup> s<sup>-1</sup>). The H $\alpha$  emission is present towards the centre of the BCG but extends  $\sim$  5'' to the southwest where it shows a second peak. *Centre Left:* The FORS2 R band image showing the BCG in A3444 with the *Chandra* X-ray map contoured over it. While the peak in the X-ray emission lies on the BCG a clear extent can be seen in the south westerly direction in the brightest emission traced by the inner most contour. *Centre Right:* The H $\alpha$  velocity field for A3444, as derived from fits to the H $\alpha$  - [NII] complex. The velocities are given relative to a redshift of z=0.2555. *Right:* The FWHM of the H $\alpha$  line emission deconvolved for instrumental resolution. The crosses mark the location of the two H $\alpha$  components on each plot. The plots are centred at RA=10:23:49.945 Dec=-27:15:25.34 (J2000). A component of H $\alpha$  emission is offset to the south west of the BCG by  $\sim$  5''. This component matches the direction of an extent in the soft X-ray emission.

masses of  $\approx 1.9 \times 10^9 M_{\odot}$  for A1991 is consistent with the correlation of molecular gas mass and optical line luminosity in Edge (2001) and with the star formation rate inferred from the MIR continuum (O’Dea et al. 2008). However, current observations cannot spatially resolve whether the star formation in the offset gas follows the correlation found for gas within the BCG (O’Dea et al. 2008).

#### 4.2 Abell 3444

A3444 also shows a substantial factor ( $\sim 63$  per cent) of optical line emission offset from the BCG. In Figure 4 we show a FORS2 *R* band image of the central region of the cluster with contours from H $\alpha$  line emission. A clear extension in the line emission can be seen to the southwest where a secondary peak is apparent. This component is offset from the BCG by  $\sim 3.2''$  or  $\sim 12.5$  kpc at the cluster redshift of 0.2533 (Struble & Rood 1999). In this cluster the line emission from the BCG and offset location are consistent within errors at  $\sim 40\%$  of the total line flux each (Table 1).

The X-ray observations of this system show a weak but significant point like source ( $L_x(0.5-10 \text{ keV}) \sim 4 \times 10^{43} \text{ ergs s}^{-1}$  in a  $1.5''$  aperture and a power law spectrum) coincident with the BCG that has a relatively hard spectrum compared to the cluster emission (Figure 5) suggesting the presence of an AGN. While the point source is centred on the BCG (Figure 4), the soft X-ray emission shows an extension in the same direction as the offset optical line emission (Figure 4) although, like A1991, it is not exactly coincident with the offset peak in the line emission.

To determine the temperature of the gas in at the location of the BCG we fit a mekal thermal plasma model (Mewe et al. 1985, 1986) to the 0.5–5.0 keV emission from a  $1.5''$  aperture centred on the BCG. This found the temperature of the gas to be  $> 7.5$  keV which is high for a plasma model suggesting a contribution to the hard X-ray emission from an AGN component. The presence of an AGN in the BCG would produce increased X-ray counts which could shift the apparent centre of the cluster emission. As such the AGN contribution must be accounted for when determining the true centre of ICM cooling.

To subtract the AGN emission from the soft X-ray emission on the BCG (and find the true level of the extended cluster emission) we determine the normalisation of the point source in the 2.0–5.0 keV band and apply this to the emission from the 0.5–1.5 keV band. To do this we first determine the properties of the cluster 2.0–5.0 keV emission from an annulus surrounding the point source. We then fit an absorbed power law plus an absorbed mekal plasma model to the point source 2.0–5.0 keV emission with the properties of the mekal component fixed to those from the surrounding annulus. Finally we apply the same model to the point source 0.5–1.5 keV emission with the normalisation and photon index of the power law set to the values determined from the Hard X-rays and calculate the flux of the two components.

The total flux from the point source in the 0.5–1.5 keV band is  $2.45_{-0.20}^{+0.24} \times 10^{-14} \text{ erg cm}^{-2} \text{ s}^{-1}$ , of which

$0.55_{-0.13}^{+0.16} \times 10^{-14} \text{ erg cm}^{-2} \text{ s}^{-1}$  comes from the AGN contribution. We find that the cluster emission under the point source is  $1.90_{-0.15}^{+0.18} \times 10^{-14} \text{ erg cm}^{-2} \text{ s}^{-1}$  while the extension to the southwest has a flux of  $2.4_{-0.12}^{+0.20} \times 10^{-14} \text{ erg cm}^{-2} \text{ s}^{-1}$  suggesting that it represents the peak in the soft X-ray emission. Analysis of the *Chandra* data also shows that the pressure in the core of A3444 is relatively constant when the AGN emission is excised. Therefore, A3444 shows very similar X-ray properties to A1991 with an offset peak in soft X-rays but a constant pressure core on 50–100 kpc scales. In the case of A3444, where the AGN in the BCG contributes significantly to the X-ray emission, the offset position in the soft X-rays represents the region of maximum cooling of the ICM.

Within this system the BCG and offset component are separated by a velocity of  $100 \pm 19 \text{ km s}^{-1}$ . We also note that the connecting emission has a higher velocity offset ( $241 \pm 26 \text{ km s}^{-1}$ ) than the offset peak. The linewidths in this system are higher in the BCG (FWHM =  $490 \pm 21 \text{ km s}^{-1}$ ) than in the offset component (FWHM =  $273 \pm 9 \text{ km s}^{-1}$ ) suggesting the gas is more disturbed within the galaxy or that it is the combination of several, related gas clouds. We also note that the lenslet from the centre of the BCG has FWHM  $> 650 \text{ km s}^{-1}$  suggesting possible contribution from the AGN detected in the X-ray imaging, that can be seen in the linewidth map in Figure 4.

In A3444, the smaller angular extent of the offset means that only a global measure of the cold molecular gas can be obtained from our IRAM observations in this system and its higher redshift restricts us to just CO(1-0). Our observation provides a marginal ( $2.0\sigma$ ) detection of  $0.33 \pm 0.11 \text{ K km s}^{-1}$  and a width of  $172 \pm 69 \text{ km s}^{-1}$  at the velocity of the BCG. However, the restricted bandwidth of the A/B100 receiver means that a broader line could be present but is lost in the baseline subtraction. The implied total molecular gas masses of  $\approx 1.7 \times 10^{10} M_{\odot}$  for A3444 is consistent with the correlation of molecular gas mass and optical line luminosity in Edge (2001).

#### 4.3 Ophiuchus

Edwards et al. (2009) studied the properties of the Ophiuchus cluster with the GMOS IFU and found line emission with a substantial ( $\sim 4''$ ) offset from the BCG (Figure 6). Edwards et al. (2009) attributed this offset line emission to another galaxy and not to the BCG itself but given the similarity with respect to the X-ray emission to A1991 and A3444 we reconsider this system. In our reanalysis of these data we also find that the line emission is offset from the BCG by  $\sim 4''$  which, at a redshift of  $z=0.028$ , corresponds to a projected separation of  $\sim 2.2$  kpc. The line emission within Ophiuchus shows no component on the BCG with 100 per cent of the H $\alpha$  emission coming from the offset component.

Million et al. (2010) also analyse *Chandra* X-ray data and find that the X-ray peak in the Ophiuchus cluster is offset from the BCG by  $\sim 4''$ , a similar offset to that seen in the line emission. In Figure 6 we compare the position of the X-rays and the offset line emission. We note that the *GMOS* field of view (shown by the dashed green

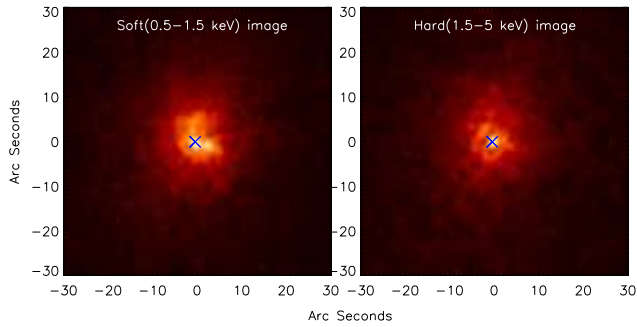


**Figure 5.** *Left* shows a soft (0.5-1.5 keV) X-ray image of the centre of A3444. A bright peak can be seen at the centre of the image which matches the position of the BCG. A secondary lower intensity peak can be seen to the west-southwest of the central peak offset by  $\sim 2$ -3 arcseconds. *Right* shows the hard (1.5-5 keV) image of the A3444 cluster core. A bright peak can clearly be seen at the centre of this image matching the position of the primary peak in the soft band. The crosses mark the location of the BCG on each image. The presence of this unresolved, hard emission on the central peak suggests this emission may be from an AGN component in the BCG.

line) ends along the north-east and north-west edges of the observed line emission but that otherwise the line emission lies towards the peak in X-ray surface brightness. While our analysis of these data find results consistent with those of Edwards et al. (2009) the alignment of the offset H $\alpha$  and X-ray emission suggests a situation similar to that in A1991 and A3444.

In this system, there is sufficient S/N in the continuum that we can determine the stellar velocity. We extracted a spectrum of the BCG and used a penalised pixel-fitting method (Cappellari & Emsellem 2004) to fit the Sodium D absorption from a catalogue of stellar templates. Comparison of the H $\alpha$  line with the Sodium D ( $\lambda$  5889,5895) stellar absorption find that the line emitting gas is offset from the BCG by  $603 \pm 28$  km s $^{-1}$ . The velocity and line width maps are shown in Figure 7, the kinematics of the gas in this system are simple although some tentative evidence for a velocity structure is apparent to the east of the object (at the edge of the GMOS field of view). Other than this the velocity of the gas shows little variation ( $\sigma = 31$  km s $^{-1}$  or half the velocity resolution of  $\sim 60$  km s $^{-1}$ ) and the linewidth is uniform across the detected line emission (FWHM =  $235 \pm 38$  km s $^{-1}$ ). Future, wider field IFU observations are required to map the full extent and velocity structure of the line emission.

#### 4.4 Time scales

The conclusion we draw from our extensive optical IFU sample (Hamer *et al.* in preparation) is that the fraction of systems in which there is an offset between the majority of the optical line emission and the central galaxy of more than 8 kpc is relatively small ( $\approx 3$  in 77). In the narrow-band imaging survey of 27 groups and clusters (McDonald et al. 2011), A1991 is the only object with

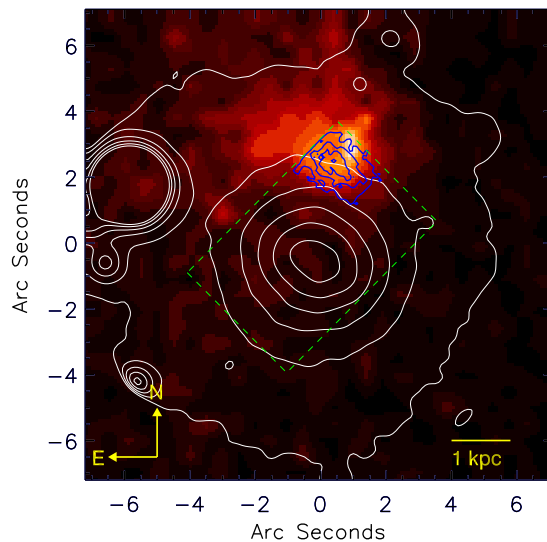


**Figure 6.** The colour scale shows the X-ray emission observed by Chandra with contours from the continuum emission from the *GMOS* R-band acquisition image of the Ophiuchus BCG. Blue contours show the position of the H $\alpha$  line emission at 6, 12, 18 and 24  $\sigma$ . The H $\alpha$  line emission is offset to the north of the BCG. The position of the offset H $\alpha$  emission lies near the peak in the X-ray surface brightness. It should be noted that the north-east and north-west edges of the line emission coincide with the edges of the *GMOS* field of view (shown as dashed green lines) so these contours may not represent the true extent of the H $\alpha$ .

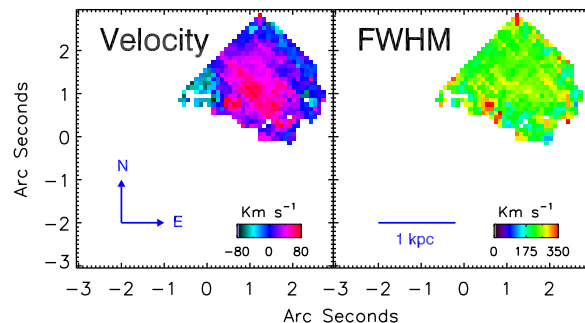


**Figure 7.** The H $\alpha$  velocity field (*Left*) and FWHM linewidth (*Right*) for Ophiuchus, as derived from fits to the H $\alpha$  - [NII] complex. The velocities are given relative to a redshift  $z=0.0304$ . The velocity and linewidths are simple and show little variation although tentative evidence for a velocity structure is apparent to the east of the object.

a second component of the optical line emission that is offset from the BCG. Similarly, from X-ray observations of 24 line emitting clusters from the LoCuSS sample (Sanderson et al. 2009) only four are offset from the X-ray centroid by more than 8 kpc (i.e. 15 per cent) (but none are offset by more than 15 kpc).

We can use the statistics of offset line emission of our sample to estimate the lifetime of such offsets. Assuming

that all clusters with a line emitting BCG may experience an offset at some stage, the fraction of BCGs showing this offset multiplied by the look-back time of the sample ( $\sim 1$  Gyr at the median redshift of our sample) gives an estimate on the lifetime of  $\sim 40$  Myr ( $3/77 \times 1$  Gyr). With IFU observations, it is also possible to estimate the lifetime of the offset using the kinematics of the gas. Assuming the offset is orientated to the line of sight at an angle  $\theta$ , the actual separation of the BCG and X-ray peak is  $D = D'/\sin\theta$ , where  $D$  is the actual separation and  $D'$  is the projected separation that we observe. Similarly the projected and actual velocity difference is given by  $V = V'/\cos\theta$ . We can determine the timescale of this separation to be  $T = D'/V' \times \cos\theta/\sin\theta$ .

Assuming that the likelihood of any orientation is uniform over the area a hemisphere, then the median orientation angle will correspond to the angle that splits the hemisphere into two equal areas. This implies that  $2\pi r^3 \cos\theta_2 = \pi r^3$  and hence  $\theta = \cos^{-1} 0.5 \sim 60^\circ$ .

A1991 has the most well constrained parameters of our three objects and therefore by setting a limit on the offset velocity and distance we can limit the range of angles over which we expect the offset to be orientated. We assume the maximum offset velocity to be  $500 \text{ km s}^{-1}$  and the offset distance to be no more than 20 kpc. These values correspond to an orientation ranging from  $\sim 30^\circ$ – $75^\circ$ . By applying the above equation with appropriate orientation angles we find that its most likely lifetime is 45 Myr with a possible range of 20–135 Myrs. These values are consistent with those calculated from the sample statistics suggesting that the lifetime of such offsets is a few tens to a hundred Myrs.

At a mass deposition rate of  $10$ – $20 M_\odot \text{ yr}^{-1}$  (Sharma et al. 2004)  $2 \times 10^7$ – $2.5 \times 10^9 M_\odot$  could condense from the ICM within 20–135 Myr. With our most likely timescale of 45 Myr this corresponds to  $5 \times 10^8$ – $10^9 M_\odot$  so the expected mass of gas is comparable to our detected CO gas mass. It should be noted that the lower mass deposition rate represents gas centred on the BCG which is at a higher temperature and lower density than that at the offset position so should be considered a lower estimate.

## 5 DISCUSSION

The most striking result from our observations is that the optical line emission is emitted predominantly from the region with the highest soft X-ray surface brightness and not the BCG. In the vast majority of clusters the peak in the X-ray emission is very close to the BCG (Peres et al. 1998; Hudson et al. 2010; Sanderson et al. 2009) so determining whether the optical lines are primarily related to the cooling of the ICM or the BCG is not possible. The direct relationship between the core X-ray properties (e.g. cooling time or entropy) and the optical line emission in any BCG has been established (Rafferty et al. 2008; Cavagnolo et al. 2008). However, only in the very small minority of clusters where the ‘sloshing’ of the ICM resulting from major or minor cluster mergers (Ascasibar & Markevitch 2006; Johnson et al. 2010; Million et al. 2010) or an episode of

strong AGN activity temporarily results in the BCG not residing at the peak of the gas cooling is there an opportunity to make the direct test of whether the optical line emission is related primarily with the cooling gas or the BCG itself.

The presence of cold molecular gas in the cores of clusters can be explained through a number of mechanisms: mergers with gas-rich cluster galaxies or gas cooling from the intracluster medium. The gas mass observed in BCGs ( $10^9$ – $11.5 M_\odot$ ) (Edge 2001; Salomé & Combes 2003) is too large to be explained by galaxy mergers or stellar mass loss but is consistent with heavily suppressed cooling from the ICM (Peterson et al. 2003; Peterson & Fabian 2006; Sanders et al. 2010).

Given the close correlation between optical lines and CO found in other cluster cores the detection of ionised gas at the location of the X-ray peak suggests the presence of a reservoir of molecular gas offset from the BCG. In A1991 and A3444 we directly detect the presence of molecular gas in the form of CO. In one system, A1991 we also detect CO at the offset position, with a molecular gas mass of  $\sim 10^9 M_\odot$ . The presence of such a high mass of molecular gas at the offset position clearly suggests that cooling is occurring despite the BCG and cluster core being separated.

Using the statistics from our sample we estimate that any offset of greater than 8 kpc can only remain for around  $10^8$  yrs. This is consistent with the dynamical timescale of the core implying that these ‘excursions’ of the BCG from the X-ray peak are short-lived. If the molecular gas at the offset position is being produced in situ then it would have to cool from the ICM within this time frame. Within the central regions of the cluster core X-ray observations predict typical cooling rates of the order  $\sim 1$ – $10 M_\odot \text{ yr}^{-1}$  (Peterson & Fabian 2006), at this rate of cooling the cluster core could deposit between  $10^8$  and  $10^9 M_\odot$  of cold molecular gas in the  $\sim 10^8$  yrs which it is not coincident with the BCG. As such, the offset molecular gas observed in A1991 is consistent with the upper band of cooling from the ICM of  $25 M_\odot \text{ yr}^{-1}$  (Sharma et al. 2004).

Although A3444 and Ophiuchus do not have separate detections of cold molecular gas at the offset position, their similarities to A1991 suggest that it may be present. Due to the smaller angular offset between BCG and X-ray peak in A3444 and Ophiuchus, resolving the molecular gas is not possible with single dish observations. However, with the start of ALMA operations there is now the possibility to directly map the molecular gas in such systems allowing the separate components of the gas to be resolved.

An alternative explanation for the morphology of the extended molecular and ionised gas is ram pressure stripping of gas related to the BCG when a merger induces large motion of the ICM relative to the BCG. This requires an efficient mechanism to entrain the dense molecular gas into the much more tenuous ICM. The effect of magnetic fields could enhance this stripping but would have to be very effective to explain the acceleration observed in Ophiuchus. The observations presented here cannot rule out ram pressure stripping. However, future mm-interferometry should be able to map the cold molec-



ular gas and allow us to distinguish between these mechanisms. If ram pressure stripping is responsible we would expect the molecular gas to be stripped less effectively than the optical line-emitting gas, while in the case of local cooling we would expect a similar morphology between the two phases.

### 5.1 Similar objects

The offset between the BCG and X-ray peak in clusters is not unique to these objects, both Abell 1644 (Johnson et al. 2010) and RXJ1347.5-1145 (Johnson et al. 2011) have a small offset and show evidence of sloshing similar to that seen here. Markevitch et al. (2003) also find that two thirds of clusters classified as cool cores by (Peres et al. 1998) show evidence of cold fronts associated with sloshing. An offset along the line of sight is not always obvious suggesting the existence of more objects in which the BCG is dissociated from the cluster core but cannot be detected by observations due to projection effects.

There are also a number of other systems where the peak of the line emission is coincident with the BCG but have less intense offset line emission in the form of extended envelopes and filaments. A1795 (Crawford et al. 2005) and RXJ0821+07 (Bayer-Kim et al. 2002) both show very extended optical emission that follows the highest X-ray emissivity in the cluster and also has associated cold molecular gas emission (Salomé & Combes 2004; Edge & Frayer 2003). Most recently, Canning et al. (2011) present evidence for a filament of optical line emission extending from the BCG in A2146 which is undergoing a major merger where the peak in the X-ray emission is offset from the BCG by 37 kpc. The IFU data presented in Canning et al. (2011) doesn't cover the X-ray peak so it can't be established if A2146 is similar to the three clusters presented here but it illustrates that a significant merger is required to dissociate the BCG from the X-ray peak. In a major merger the disruption in the core will be significant. Russell et al. (2010) show that the pressure profile in the core of A2146 is very asymmetric, unlike that in A1991 which is dynamically more quiescent. Therefore, the process of cluster-cluster merging, and the longer lived sloshing that it induces, may be required to produce the brief decoupling of the peak in the intracluster medium density from the BCG observed in all of these systems.

Another viable mechanism for inducing bulk motion of the ICM in a cluster core is the inflation of cavities due to AGN activity in the BCG. Blanton et al. (2011) show a close correspondance between filaments of high X-ray surface brightness and optical line emission in A2052 which has an extensive cavity network. The compressed gas in these filaments has a short cooling time so the optical line emission may also be related to local cooling. The systems presented in this paper do not resemble A2052 or exhibit the large cavities required to generate the observed offsets, so AGN feedback is unlikely to explain the lop-sided offsets we observe in A1991, A3444 and Ophiuchus. However, the small scale correlation be-

tween strongest X-ray cooling and optical line emission suggests a common mechanism behind them.

The existence of cold gas that is 'orphaned' in the cores of clusters may have a number of implications for more distant systems. For instance, in the high redshift radio galaxy TXS0828+193 ( $z = 2.6$ ), Nesvadba et al. (2009) find a cloud of cold molecular gas emitting at CO(3-2) that has no bright optical or near-infrared counterpart that is 80 kpc from the radio galaxy itself. They speculate that this may be analogous to low redshift clusters but note that the gas tends to be associated with the central galaxy. While the total gas mass and physical offset are substantially larger in TXS0828+193 than in A1991 or A3444, the similarity between the systems may point to a common mechanism.

## 6 SUMMARY

Within the cores of most clusters there is a clear spatial coincidence between the position of the BCG and the peak of the ICM density. However there are a few clusters in which the BCG and cluster core are found to be decoupled. In such systems, it is possible to disentangle the effects of the cluster core and the BCG on the ICM and study each individually. Here we study three such systems selected from a parent sample of 77 massive X-ray selected clusters where we find that the optical, millimetre and X-ray observations of the cores show extended optical line emission and cold molecular gas directly related to the peak of the cooling of the intracluster medium and not the central galaxy. These three systems are the only clusters from our sample to show a significant offset between the BCG and cluster core suggesting that such a phenomenon is rare and transient. From our sample we find that a significant offset occurs in only 2–3 per cent of systems and that they likely have lifetimes lasting of the order of 20–100 Myr. We note however that it is possible for systems to have an offset along the line of sight which we would not detect so this fraction may be slightly higher and should be considered a lower limit.

The rarity of such significant offsets between the BCG, X-ray peak and optical line emission points to a large event in cluster evolution, a major cluster merger or possibly a powerful AGN outburst. Mergers are predicted to drive shocks through the core of the ICM at early times and cause sloshing as a later effect (Ascasibar & Markevitch 2006; Johnson et al. 2010; Million et al. 2010; ZuHone et al. 2010; ZuHone 2011) both of which are capable of separating the BCG from the cluster core. X-ray observations of A1991 suggest the passage of a cluster-wide shock through the core of the cluster and similar observations of Ophiuchus show sloshing of the ICM suggesting the possibility of a recent merger. Whatever the reason for the separation the gas cooling at the X-ray peak will continue and cooled gas will be deposited away from the BCG. This provides a unique opportunity to directly constrain the process of gas cooling without the presence of a BCG.

**ACKNOWLEDGEMENTS**

SLH acknowledges the support received from an STFC studentship. AMS acknowledges an STFC Advanced Fellowship. HRR acknowledges generous financial support from the Canadian Space Agency Space Science Enhancement Program. ACF thanks the Royal Society for support.

Based on observations made with ESO Telescopes at the La Silla or Paranal Observatories under programme ID 081.A-0422 and 385.A-0955.

Based on observations carried out with the IRAM 30m Telescope. IRAM is supported by INSU/CNRS (France), MPG (Germany) and IGN (Spain)

Based on observations obtained at the Gemini Observatory, which is operated by the Association of Universities for Research in Astronomy, Inc., under a cooperative agreement with the NSF on behalf of the Gemini partnership: the National Science Foundation (United States), the Science and Technology Facilities Council (United Kingdom), the National Research Council (Canada), CONICYT (Chile), the Australian Research Council (Australia), Ministerio de Ciencia, Tecnología e Innovación (Brazil) and Ministerio de Ciencia, Tecnología e Innovación Productiva (Argentina).

**REFERENCES**

- Ascasibar Y., Markevitch M., 2006, *ApJ*, 650, 102  
 Bayer-Kim C. M., Crawford C. S., Allen S. W., Edge A. C., Fabian A. C., 2002, *MNRAS*, 337, 938  
 Blanton E. L., Randall S. W., Clarke T. E., Sarazin C. L., McNamara B. R., Douglass E. M., McDonald M., 2011, *ApJ*, 737, 99  
 Canning R. E. A., Russell H. R., Hatch N. A., Fabian A. C., Zabludoff A. I., Crawford C. S., King L. J., McNamara B. R., et al. 2011, *MNRAS* in press, arXiv:1111.0452  
 Cappellari M., Emsellem E., 2004, *PASP*, 116, 138  
 Cavagnolo K. W., Donahue M., Voit G. M., Sun M., 2008, *ApJ*, 683, L107  
 Crawford C. S., Allen S. W., Ebeling H., Edge A. C., Fabian A. C., 1999, *MNRAS*, 306, 857  
 Crawford C. S., Sanders J. S., Fabian A. C., 2005, *MNRAS*, 361, 17  
 Ebeling H., Edge A. C., Bohringer H., Allen S. W., Crawford C. S., Fabian A. C., Voges W., Huchra J. P., 1998, *MNRAS*, 301, 881  
 Edge A. C., 2001, *MNRAS*, 328, 762  
 Edge A. C., Frayer D. T., 2003, *ApJ*, 594, L13  
 Edge A. C., Stewart G. C., 1991a, *MNRAS*, 252, 428  
 Edge A. C., Stewart G. C., 1991b, *MNRAS*, 252, 414  
 Edwards L. O. V., Robert C., Mollá M., McGee S. L., 2009, *MNRAS*, 396, 1953  
 Fabian A. C., 1994, *ARA&A*, 32, 277  
 Fabian A. C., Hu E. M., Cowie L. L., Grindlay J., 1981, *ApJ*, 248, 47  
 Fabian A. C., Johnstone R. M., Sanders J. S., Conselice C. J., Crawford C. S., Gallagher III J. S., Zweibel E., 2008, *Nature*, 454, 968  
 Hatch N. A., Crawford C. S., Fabian A. C., Johnstone R. M., 2005, *MNRAS*, 358, 765  
 Hatch N. A., Crawford C. S., Johnstone R. M., Fabian A. C., 2006, *MNRAS*, 367, 433  
 Hudson D. S., Mittal R., Reiprich T. H., Nulsen P. E. J., Andernach H., Sarazin C. L., 2010, *A&A*, 513, A37+  
 Johnson R. E., Markevitch M., Wegner G. A., Jones C., Forman W. R., 2010, *ApJ*, 710, 1776  
 Johnson R. E., ZuHone J. A., Jones C., Forman W., Markevitch M., 2011, *ArXiv e-prints*  
 Lahav O., Fabian A. C., Edge A. C., Putney A., 1989, *MNRAS*, 238, 881  
 Markevitch M., Vikhlinin A., Forman W. R., 2003, in S. Bowyer & C.-Y. Hwang ed., *Astronomical Society of the Pacific Conference Series Vol. 301 of Astronomical Society of the Pacific Conference Series, A High Resolution Picture of the Intracluster Gas*. pp 37+  
 McDonald M., Veilleux S., Mushotzky R., 2011, *ApJ*, 731, 33  
 Mewe R., Gronenschild E. H. B. M., van den Oord G. H. J., 1985, *A&AS*, 62, 197  
 Mewe R., Lemen J. R., van den Oord G. H. J., 1986, *A&AS*, 65, 511  
 Million E. T., Allen S. W., 2009, *MNRAS*, 399, 1307  
 Million E. T., Allen S. W., Werner N., Taylor G. B., 2010, *MNRAS*, 405, 1624  
 Nesvadba N. P. H., Neri R., De Breuck C., Lehnert M. D., Downes D., Walter F., Omont A., Boulanger F., Seymour N., 2009, *MNRAS*, 395, L16  
 O’Dea C. P., Baum S. A., Maloney P. R., Tacconi L. J., Sparks W. B., 1994, *ApJ*, 422, 467  
 O’Dea C. P., Baum S. A., Privon G., Noel-Storr J., Quillen A. C., Zufelt N., Park J., Edge A., et al. 2008, *ApJ*, 681, 1035  
 Peres C. B., Fabian A. C., Edge A. C., Allen S. W., Johnstone R. M., White D. A., 1998, *MNRAS*, 298, 416  
 Peterson J. R., Fabian A. C., 2006, *Phys. Rep.*, 427, 1  
 Peterson J. R., Kahn S. M., Paerels F. B. S., Kaastra J. S., Tamura T., Bleeker J. A. M., Ferrigno C., Jernigan J. G., 2003, *ApJ*, 590, 207  
 Rafferty D. A., McNamara B. R., Nulsen P. E. J., 2008, *ApJ*, 687, 899  
 Russell H. R., Sanders J. S., Fabian A. C., Baum S. A., Donahue M., Edge A. C., McNamara B. R., O’Dea C. P., 2010, *MNRAS*, 406, 1721  
 Salomé P., Combes F., 2003, *A&A*, 412, 657  
 Salomé P., Combes F., 2004, *A&A*, 415, L1  
 Salomé P., Combes F., Edge A. C., Crawford C., Erlund M., Fabian A. C., Hatch N. A., Johnstone R. M., et al. 2006, *A&A*, 454, 437  
 Salomé P., Combes F., Revaz Y., Downes D., Edge A. C., Fabian A. C., 2011, *A&A*, 531, A85+  
 Sanders J. S., Fabian A. C., Frank K. A., Peterson J. R., Russell H. R., 2010, *MNRAS*, 402, 127  
 Sanderson A. J. R., Edge A. C., Smith G. P., 2009, *MNRAS*, 398, 1698  
 Schombert J. M., 1987, *ApJS*, 64, 643  
 Schombert J. M., 1988, *ApJ*, 328, 475  
 Sharma M., McNamara B. R., Nulsen P. E. J., Owers M., Wise M. W., Blanton E. L., Sarazin C. L., Owen F. N., et al. 2004, *ApJ*, 613, 180

- Struble M. F., Rood H. J., 1999, *ApJS*, 125, 35  
Tremaine S., 1990, The origin of central cluster galaxies..  
pp 394–405  
Wilman R. J., Edge A. C., Swinbank A. M., 2006, *MNRAS*, 371, 93  
ZuHone J. A., 2011, *ApJ*, 728, 54  
ZuHone J. A., Markevitch M., Johnson R. E., 2010, *ApJ*,  
717, 908